

Highly Sensitive and Fast Responsive Fluorescence Turn-On Chemodosimeter for Cu²⁺ and Its Application in Live Cell Imaging

Mengxiao Yu,^[a] Mei Shi,^[a] Zhigang Chen,^[a] Fuyou Li,^{*[a]} Xinxin Li,^[b] Yanhong Gao,^[c] Jia Xu,^[a] Hong Yang,^[a] Zhiguo Zhou,^[a] Tao Yi,^[a] and Chunhui Huang^{*[a]}

Abstract: A rhodamine B derivative **4** containing a highly electron-rich S atom has been synthesized as a fluorescence turn-on chemodosimeter for Cu²⁺. Following Cu²⁺-promoted ring-opening, redox and hydrolysis reactions, comparable amplifications of absorption and fluorescence signals were observed upon addition of Cu²⁺; this suggests that chemodosimeter **4** effectively avoided the fluorescence quenching caused by the paramagnetic nature of Cu²⁺. Importantly, **4** can selectively

recognize Cu²⁺ in aqueous media in the presence of other trace metal ions in organisms (such as Fe³⁺, Fe²⁺, Cu⁺, Zn²⁺, Cr³⁺, Mn²⁺, Co²⁺, and Ni²⁺), abundant cellular cations (such as Na⁺, K⁺, Mg²⁺, and Ca²⁺), and the prevalent toxic metal ions in the environment (such as Pb²⁺ and Cd²⁺) with

high sensitivity (detection limit ≤10 ppb) and a rapid response time (≤1 min). Moreover, by virtue of the chemodosimeter as fluorescent probe for Cu²⁺, confocal and two-photon microscopy experiments revealed a significant increase of intracellular Cu²⁺ concentration and the subcellular distribution of Cu²⁺, which was internalized into the living HeLa cells upon incubation in growth medium supplemented with 50 μM CuCl₂ for 20 h.

Keywords: chemodosimeter • copper • fluorescent probes • imaging agents • rhodamine

Introduction

Copper, after iron and zinc, is the third most abundant essential trace element in the human body, and plays an important role in many fundamental physiological processes in organisms.^[1] Alteration in the cellular homeostasis of copper

ions is associated with some serious neurodegenerative diseases, including Menkes and Wilson diseases,^[2] Alzheimer's disease,^[3] familial amyotrophic lateral sclerosis,^[4] and prion diseases.^[5] In particular, exposure to a high level of copper even for a short period of time can cause gastrointestinal disturbance, and long-term exposure causes liver or kidney damage,^[6] as a result of its ability to displace other metal ions that act as cofactors in enzyme-catalyzed reactions.^[7] Thus, visualizing the concentration and subcellular distribution of copper in physiological processes may greatly contribute to understanding its complex physiological functions and nosogenesis.

By virtue of its highly sensitive and high-speed spatial analysis of cells, fluorescence bioimaging has provided a facile and less cell-damaging means of visualizing analytes of biological interest in living cells.^[8,9] To image intracellular metal ions, highly sensitive and selective probes that exhibit an enhanced visible fluorescent emission in aqueous media need to be developed. A widely used strategy is to closely link the metal recognition portion to a fluorophore as the signal generation moiety and then a selective metal ion binding process could induce the fluorescence increase. In this way, several "turn-on" fluorescent probes in living cells for sensing main Group II metal ions (such as Ca²⁺ and Mg²⁺)^[10] and transition-metal ions (such as Zn²⁺,^[11,12]

[a] M. Yu, Dr. M. Shi, Z. Chen, Prof. F. Li, J. Xu, H. Yang, Z. Zhou, Prof. T. Yi, Prof. C. Huang
Department of Chemistry & Laboratory of Advanced Materials
Fudan University, 220 Handan Road, Shanghai 200433 (PR China)
Fax: (+86)21-5566-4621
E-mail: fyl@fudan.edu.cn
chhuang@fudan.edu.cn

[b] Prof. X. Li
School of Materials Science and Engineering
East China University of Science and Technology
130 Meilong Road, Shanghai 200237 (PR China)

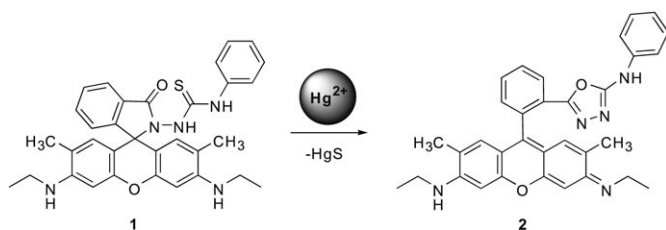
[c] Dr. Y. Gao
Hospital of Xinhua, Medicine School of Shanghai Jiaotong University
1665 Kongjiang Road, Shanghai 200092 (PR China)

Supporting information for this article is available on the WWW under <http://dx.doi.org/10.1002/chem.200800005>: UV/Vis and fluorescence spectra, charge numbers of atoms in **1** and **4**, ESI mass spectra, XPS spectrum, fluorescence images, the result of trypan blue viability test and the other supplementary materials, including colour versions of Figure 5, Scheme 3, and Table 1.

Cd²⁺,^[13] Cu⁺,^[14] Pb²⁺,^[15] Fe³⁺,^[16] and Hg²⁺^[17]) have been successfully designed and synthesized. However, this method has been applied to Cu²⁺ with only limited success.^[18,19] Due to the intrinsic fluorescence quenching property that stems from the paramagnetic nature of Cu²⁺,^[20] most hitherto reported Cu²⁺ sensors have shown decreased emission upon Cu²⁺ binding.^[18] Such fluorescence “turn-off” sensors may give false positive results caused by other quenchers in real samples and are undesirable for analytical purposes. In addition, although few fluorescence “turn-on” Cu²⁺ sensors^[19] with nanomolar sensitivity,^[19a-c,g] high selectivity,^[19a,g] rapid response, or good water solubility^[19g] have been reported, sensors which combine all these features have not been obtained up until now. Based on the above reasons, to the best of our knowledge, no work on fluorescence bioimaging of Cu²⁺ has previously been reported. Thus, the development of highly sensitive turn-on fluorescent probes for monitoring Cu²⁺ in living cells still remains a significant challenge.

To date, the chemodosimeter has attracted a tremendous amount of attention as an alternative to sensors based on metal ion binding mechanism mentioned above due to its high sensitivity and a rapid response.^[21,22] Chemodosimeter indicates the presence of an analyte through the generation of a fluorescent or colored product resulting from a specific chemical reaction between the dosimeter molecule and the target species. In particular, the chemodosimeter provides an ideal way to design fluorescence “turn-on” probes for paramagnetic metal ions such as Cu²⁺, since the fluorescent product does not coordinate to metal ions. However, the lack of highly selective reactions induced by Cu²⁺, which occur fast in aqueous solution at room temperature, remain a big hurdle for obtaining such probes. Based on a Cu²⁺-promoted hydrolysis reaction of rhodamine hydrazide, Czarnek et al. designed a chemodosimeter for Cu²⁺ in water,^[21] although its ability to sense Cu²⁺ in cells was not investigated. Recently, Tae et al. reported that a rhodamine 6G derivative **1** was capable of serving as a chemodosimeter for Hg²⁺.^[23] This derivative responds to Hg²⁺ stoichiometrically, rapidly, and irreversibly at room temperature through desulfurization and cyclization reactions which produce a strongly fluorescent product **2** (Scheme 1).

Inspired by such a chemodosimeter for Hg²⁺, we surmised that a marked increase of the electronegativity of the S atom could lead to similar reactions being induced by other sulfophilic elements, such as copper. In the present work, a

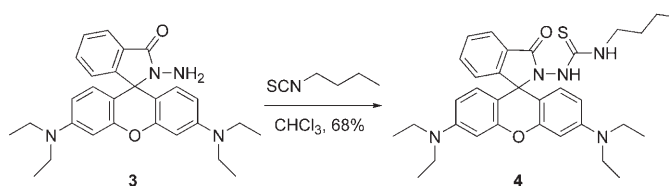


Scheme 1. Conversion of nonfluorescent **1** to strongly fluorescent **2** by Hg²⁺.

rhodamine B derivative **4** containing a highly electron-rich S atom has been demonstrated as a chemodosimeter for Cu²⁺. Furthermore, confocal and two-photon fluorescence microscopy experiments have demonstrated that **4** can be used to image Cu²⁺ in living cells.

Results and Discussion

Synthesis and characterization of 4: Probe **4** was easily synthesized in 68% yield by a condensation reaction of rhodamine B hydrazide (**3**) and *n*-butyl isothiocyanate (Scheme 2). The structure of **4** was confirmed by ¹H NMR,



Scheme 2. Chemical structure and synthetic routine of **4**.

¹³C NMR spectroscopic, and MS data and by single-crystal X-ray diffraction analysis. A single crystal of **4** was obtained by slow evaporation of the solvent from a solution in CH₃CN. The single-crystal X-ray diffraction study reveals that the molecules of **4** adopt a spirocyclic form in the crystal (Figure 1). The butyl group is split between two locations with equal occupancies, reflecting its propensity to swing in the crystal.

A solution of **4** in CH₃CN or CH₃CN/HEPES (50 mM, pH 7.2, 3:7, v/v) solution was colorless and weakly fluorescent, indicating that the spirocyclic form was retained in solution. The characteristic peak at δ =67.0 ppm in the ¹³C NMR spectrum of **4** also supported this conclusion.

Hg²⁺/Cu²⁺ response of 4: Based on the well-known equilibrium between non-fluorescent spirolactam and the fluorescent ring-opened amide of rhodamine,^[16,17d,25] it is reasoned that **4** with a thiourea group can be used as a fluorescent probe for soft metal ions. Since **4** is similar in chemical structure to **1**, the response of **4** to Hg²⁺ was investigated by UV/Vis absorption and fluorescence spectra. Interestingly, the behavior of **4** in sensing Hg²⁺ was distinct from that of **1** in response to Hg²⁺. Tae et al.^[23] described that the fluorescence intensity of **1** was nearly proportional to the Hg²⁺ concentration when up to one equivalent of Hg²⁺ was added. In our case, a weak increase in the absorption and emission of **4** was observed upon addition of less than one equivalent of Hg²⁺, as shown in Figure 2. Further addition of Hg²⁺ caused a significant increase in the absorption band centered at 566 nm and fluorescent emission peaked at 591 nm (see Figures S1 and S2 in the Supporting Information), corresponding to the appearance of a purple-red color and an intense orange-red fluorescence. These facts imply

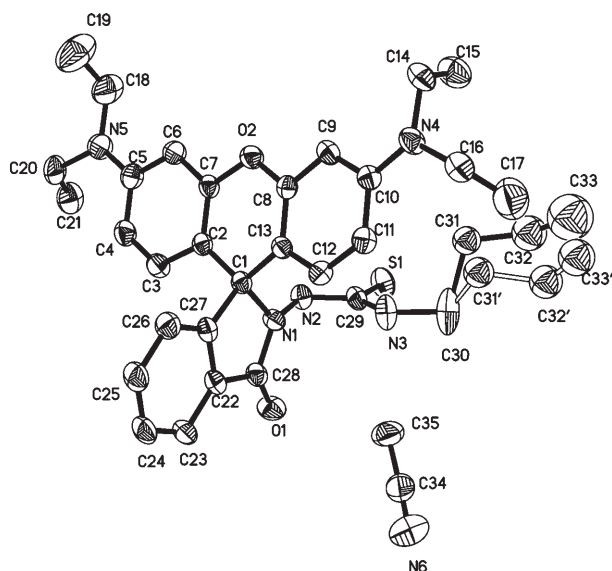


Figure 1. ORTEP drawing of **4** (30% ellipsoid). H atoms are omitted for clarity.^[24]

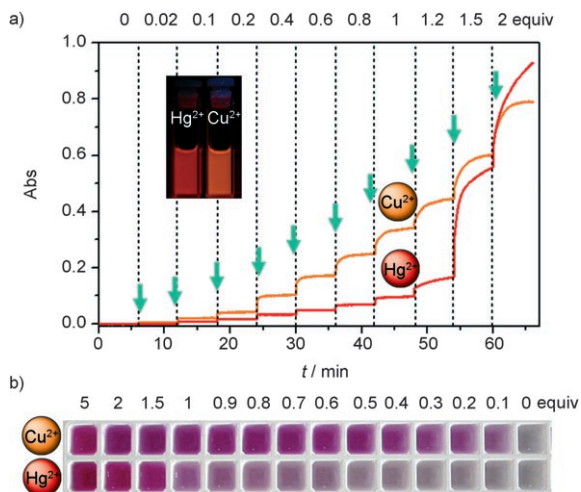


Figure 2. Distinct difference in Cu^{2+} and Hg^{2+} sensing behavior of **4** in $\text{CH}_3\text{CN}/\text{HEPES}$ (50 mM, pH 7.2, 3:7, v/v) solution. a) Time course of 20 μM **4** upon gradual addition of Cu^{2+} and Hg^{2+} . Absorbance at 555 nm (for Cu^{2+}) and 566 nm (for Hg^{2+}) was recorded respectively. Inset shows the fluorescent responses of **4** to 5 equiv of Cu^{2+} and Hg^{2+} under 365 nm UV excitation. b) Color changes of 20 μM **4** in the presence of different concentrations of Cu^{2+} or Hg^{2+} .

that **4** might show a distinct recognition of metal ions as compared to **1**.

More interestingly, unlike **1**, **4** can also respond to Cu^{2+} . When Cu^{2+} was gradually added to a solution of **4**, a new absorption band with a maximum at 555 nm appeared, corresponding to the observation of a new emission band centered at 580 nm (Figure S3 in the Supporting Information). Unlike the response of **4** to Hg^{2+} , a proportional increase in absorption and emission was observed in its sensing of Cu^{2+} (Figure 2 and Figure S3 in the Supporting Information). It is worthy of note that the fluorescent color of **4** in the pres-

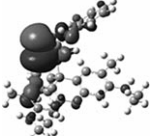
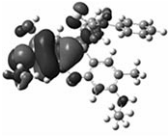
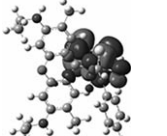
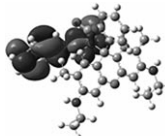
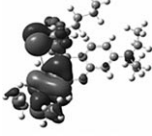
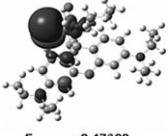
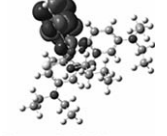
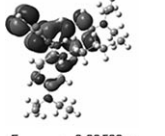
ence of Cu^{2+} was distinct from that of **4** upon addition of Hg^{2+} (the inset of Figure 2a). The emission maximum of the mixture of **4** and Hg^{2+} ($\lambda_{\text{max}}^{\text{em}} = 591 \text{ nm}$) was red-shifted by $\approx 10 \text{ nm}$ in comparison with that of **4** in response to Cu^{2+} ($\lambda_{\text{max}}^{\text{em}} = 580 \text{ nm}$), possibly indicating different products of **4** in the sensing of Cu^{2+} and Hg^{2+} . Moreover, the intense fluorescence of **4** induced by Hg^{2+} or Cu^{2+} could not be suppressed by further addition of excess chelating agent, such as EDTA (see Figures S4 and S5 in the Supporting Information), which suggests irreversible sensing processes of **4** in response to these metal ions.

Recognition mechanism of **4 towards $\text{Hg}^{2+}/\text{Cu}^{2+}$:** To understand the different recognition abilities of **1** and **4** towards Cu^{2+} , the HOMO and LUMO distributions of **1** and **4** were determined by density functional theory (DFT) calculations. As shown in Table 1, the HOMO distribution of **4** is concentrated exclusively on the S atom of the thiourea group, while that of **1** is located diffusely over the thiourea and xanthene moieties. This result reveals that the introduction of the *n*-butyl group significantly increased the HOMO electron density on the S atom. Furthermore, the charge on the S atom in **4** is -0.20 , whereas in **1** it is -0.16 (see Figures S6 and S7 in the Supporting Information). In the metal ion promoted desulfurization reaction, the S atom of **4** becomes an electron-rich center and exhibits a higher affinity for the metal ion. Thus, the HOMO distribution exclusively on the S atom of **4** and the increased electronegativity would constitute a reason for its unique response to Cu^{2+} .

We further investigated the final reaction products of **4** with Cu^{2+} and Hg^{2+} by ESI mass spectrometry. The ESI mass spectrum of **4** with two equiv Hg^{2+} showed a unique peak at m/z 538.3 (calcd for 538.3) (see Figure S8 in the Supporting Information), corresponding to a desulfurized and cyclized product [**5**]⁺ (Scheme 3). In the case of **4** with two equiv Cu^{2+} , a peak at m/z 443.2 (calcd for 443.3) assigned to [**6**]⁺ (namely rhodamine B, see Scheme 3) was clearly observed (see Figure S9 in the Supporting Information). Corroborating evidence was provided by independent syntheses of **5** and **6** from the direct reactions of **4** with $\text{Hg}(\text{ClO}_4)_2$ and $\text{Cu}(\text{NO}_3)_2$, respectively, in CH_3CN at room temperature; ¹H NMR and MS data confirmed their structures. These results indicate a distinct recognition mechanism of **4** towards Cu^{2+} as compared to that of its response to Hg^{2+} .

Recently, Chorev et al.^[26] have reported that dialkyl-substituted thioureas undergo rapid formation of the intermediate carbodiimide in the presence of $\text{Hg}(\text{OAc})_2$ (Scheme 4). Thus, we can deduce a recognition mechanism of **4** towards Hg^{2+} as follows (Scheme 3): a) In the presence of less than one equiv Hg^{2+} , **4** undergoes an irreversible desulfurization reaction and is thereby converted into an intermediate carbodiimide **7**, in accordance with the observations of Chorev et al.^[26] This is further confirmed by the appearance of a peak at m/z 538.2 (calcd for 538.3) assigned to [**7**+H]⁺ in the ESI mass spectrum of a colorless and weakly fluorescent mixture of **4** with 0.5 equiv of Hg^{2+} in ethanol (see Figure S10 in the Supporting Information). The weak increase in

Table 1. HOMO–1, HOMO, LUMO and LUMO+1 distributions of **1** and **4** calculated by DFT calculations.

	HOMO-1	HOMO	LUMO	LUMO+1
1	 $E_{\text{HOMO-1}} = -0.18592\text{eV}$	 $E_{\text{HOMO}} = -0.18132\text{eV}$	 $E_{\text{LUMO}} = -0.03477\text{eV}$	 $E_{\text{LUMO+1}} = -0.01653\text{eV}$
2	 $E_{\text{HOMO-1}} = -0.17811\text{eV}$	 $E_{\text{HOMO}} = -0.17688\text{eV}$	 $E_{\text{LUMO}} = -0.02684\text{eV}$	 $E_{\text{LUMO+1}} = -0.00593\text{eV}$

absorption and fluorescence indicates that the molecules of **7** adopt a spiro lactam form. b) Upon further addition of more than one equiv Hg^{2+} , the ring-opened product **5** containing a 1,3,4-oxadiazole moiety is formed by an Hg^{2+} -promoted cyclization reaction, resulting in an obvious absorption and fluorescence enhancement.

In the case of copper, although Cu^+ does not induce the response of **4** (see Figure S11 in the Supporting Information), the Cu 2p X-ray photoelectron spectra (XPS) analyses demonstrate the presence of Cu^+ . In the mixture of **4** with 0.5 equiv Cu^{2+} , the peaks having binding energies of 932.2 and 951.8 eV, corresponding to Cu 2p_{3/2} and 2p_{1/2} of Cu^+ , respectively, were observed (see Figure S12 in the Supporting Information). In addition, the S atom of the thiourea group in **4** shows higher electronegativity as compared to that in **1**. Based on these facts, the mechanism of Cu^{2+} induced fluorescence increase of **4** can be proposed as follows (Scheme 3): c) A Cu^{2+} -promoted ring-opening reaction of **4** occurs instantly upon the addition of Cu^{2+} , owing to the strong binding ability of the O, N, and S atoms towards Cu^{2+} . d) Due to the rather electron-rich rhodamine–thiourea moiety as electron donor, a redox reaction between **4** and Cu^{2+} could occur, thus reducing Cu^{2+} to Cu^+ . A peak at m/z 634.2 (calcd for 634.2) assigned to an intermediate **8** including a Cu^+ was evident from the ESI mass spectrum of **4** with 0.5 equiv Cu^{2+} in ethanol. The peaks at m/z 1205.4 (calcd for 1205.5), 1268.3 (calcd for 1268.5), 1331.2 (calcd for 1331.4), which could be identified as a series of intermediates such as CuL_2 , Cu_2L_2 , Cu_3L_2 (L stands for the ligand **4**) were also detected (see Figure S13 in the Supporting Information). e) Subsequently, a further hydrolysis occurs, resulting in the formation of the final product **6**, which exhibits intense photoluminescence. In aqueous media, the Cu^{2+} -promoted ring-opening, redox and hydrolysis reactions described above happen rapidly, therefore, one can observe a continuous variation in the absorption and fluorescence spectra when Cu^{2+} is gradually added (Figure 2). Naturally, a peak at m/z 538.2 in the ESI mass spectrum of the mixture of **4** with Cu^{2+} (see Figure S13 in the Supporting Information) implies that another recogni-

tion process similar to that of its response to Hg^{2+} occurred possibly for **4** response to Cu^{2+} .

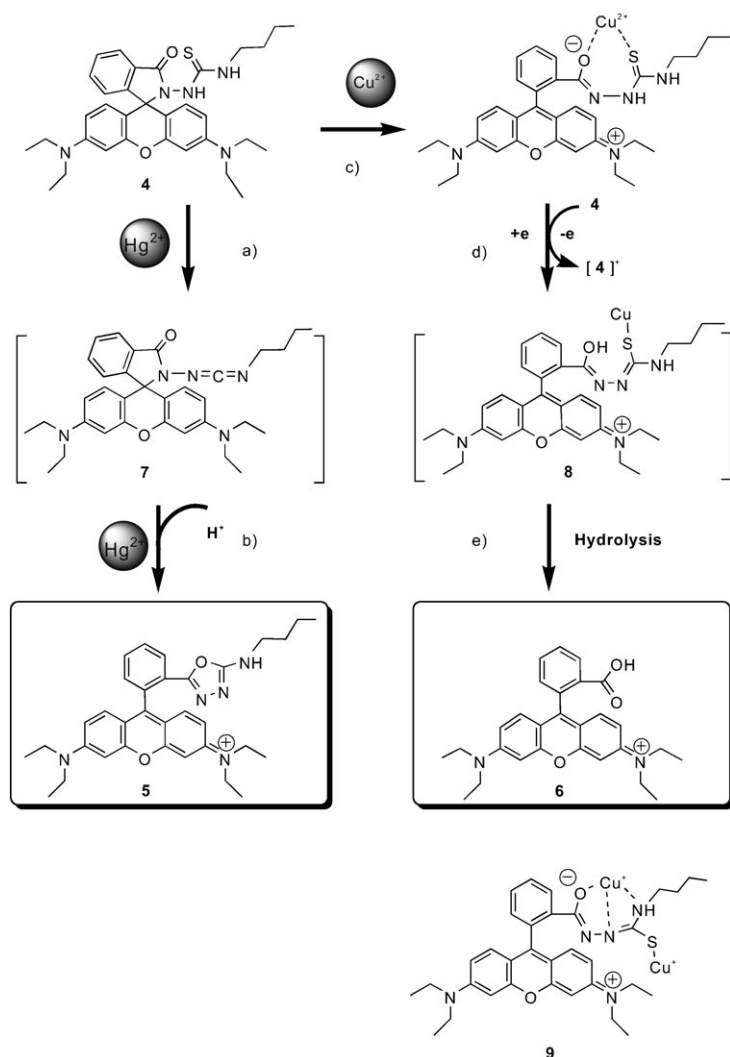
Detection of Cu^{2+} in vitro: In view of the absence of Hg^{2+} in normal living samples, the possibility of using **4** as a fluorescent probe for monitoring intracellular Cu^{2+} was also investigated. Such a similar treatment is commonly used in the case of Zn^{2+} bioimaging by Zn^{2+} -selective fluorescent sensors with interference from Cd^{2+} .^[12a,b] The pH dependence of the Cu^{2+}

sensing by **4** was determined. No obvious fluorescence emission of **4** was observed between pH 4.8 and 11.8, suggesting that the compound is stable over a wide range. In the range pH 5.8–8.8, a marked fluorescence enhancement was measured upon addition of Cu^{2+} (see Figure S14 in the Supporting Information). These data establish that **4** could act as a fluorescent probe for Cu^{2+} under physiological pH conditions.

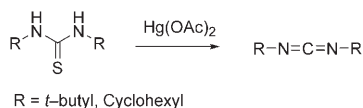
In absorption and fluorescence titrations of 20 μM **4** in $\text{CH}_3\text{CN}/\text{HEPES}$ (50 mM, pH 7.2, 3:7, v/v) solution, a 430-fold increase in the absorbance at 555 nm was observed upon addition of 5 equiv Cu^{2+} (Figure 3) and a comparable fluorescence enhancement (470-fold) at 580 nm was also detected ($\Phi_f = 0.31$); this suggests that the chemodosimeter effectively avoided the fluorescence quenching caused by the paramagnetic nature of Cu^{2+} . Moreover, to assess the possibility of detecting Cu^{2+} at a low concentration, fluorescence titrations were conducted with 1 μM **4**. The fluorescence intensity was found to increase linearly with the Cu^{2+} concentration in the range of 4.5–160 ppb (Figure 4). The detection limit of this chemodosimeter system was estimated to be 10 ppb (Figure 4b), which is comparable to those of some previously reported highly sensitive sensors.^[19a–c,g] In addition, different copper salts, such as CuCl_2 , $\text{Cu}(\text{NO}_3)_2$, and CuSO_4 , gave rise to the same fluorescence profiles in its response to Cu^{2+} (see Figure S15 in the Supporting Information), indicating a negligible effect of the counteranions on the recognition ability and photophysical properties of **4**.

Furthermore, the time dependence of the response of **4** to Cu^{2+} was monitored by means of absorption spectroscopy (Figure 5). The results revealed that the reaction of 20 μM **4** and Cu^{2+} ($\leq 100 \mu\text{M}$) was complete within 1 min. In particular, an instantaneous response towards Cu^{2+} at low concentrations ($\leq 1 \mu\text{M}$) was observed. Therefore, this system could be used for real-time tracking of Cu^{2+} in cells and organisms.

Achieving high selectivity for the analyte of interest over other potentially competing species is a necessity for bioimaging probes. Thus, the selectivity and competition experiments were extended to various metal ions, such as abundant cellular cations (Na^+ , K^+ , Mg^{2+} , and Ca^{2+}), trace



Scheme 3. Proposed mechanisms for Hg^{2+} and Cu^{2+} -promoted fluorescence enhancement of **4**. a) Hg^{2+} -triggered desulfurization reaction to produce an intermediate carbodiimide **7** with weakly fluorescence. b) Hg^{2+} -induced ring-opening of the spiro lactam and cyclization reaction of **7**, resulting in the formation of fluorescent product **5**. c) Cu^{2+} -promoted ring-opening reaction of **4**, owing to the strong binding ability of the O, N, and S atoms towards Cu^{2+} . d) Redox reaction between Cu^{2+} and **4**, due to the rather electron-rich rhodamine-thiourea moiety as electron donor. An intermediate **8** including a Cu^+ is demonstrated by the ESI mass spectrum analyses. e) Hydrolysis reaction in aqueous media, producing the final product **6** (namely rhodamine B).



Scheme 4. Formation of intermediate carbodiimide from a 1,3-dialkylthiourea.^[26]

metals in organisms (Fe^{3+} , Fe^{2+} , Cu^{2+} , Cu^+ , Zn^{2+} , Cr^{3+} , Mn^{2+} , Co^{2+} , and Ni^{2+}), and the prevalent toxic metals in the environment (Pb^{2+} and Cd^{2+}). As shown in Figure 6,

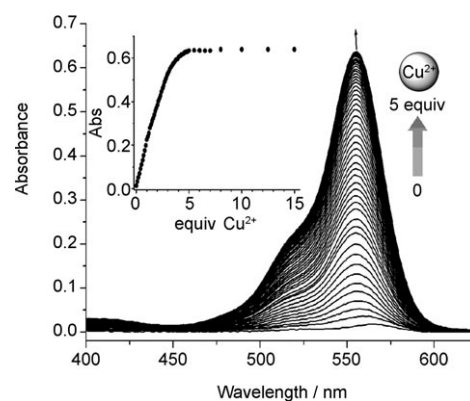


Figure 3. Absorption spectra of $20 \mu\text{M}$ **4** upon addition of Cu^{2+} in $\text{CH}_3\text{CN}/\text{HEPES}$ (50 mM, pH 7.2, 3:7, v/v) solution. Inset shows the absorbance at 555 nm of **4** as a function of Cu^{2+} concentration.

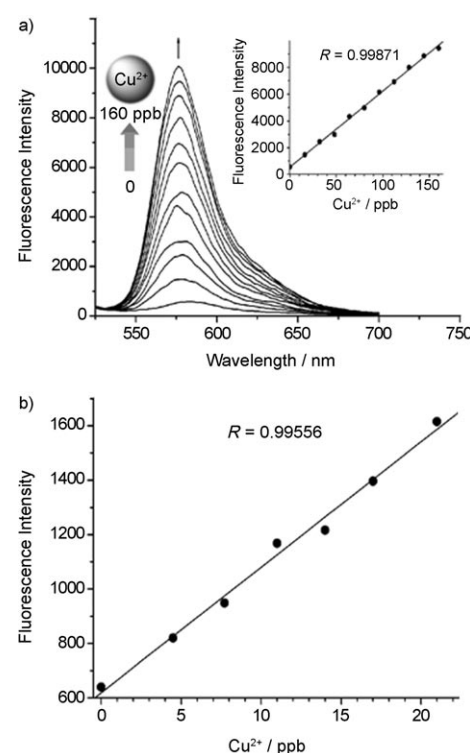


Figure 4. Fluorescence responses of $1 \mu\text{M}$ **4** upon addition of 4.5–160 ppb Cu^{2+} in $\text{CH}_3\text{CN}/\text{HEPES}$ (50 mM, pH 7.2, 3:7, v/v) solution. Inset and b) show the fluorescence intensity at 580 nm of **4** as a function of Cu^{2+} concentration (inset of a) 0–160 ppb; b) 0–21 ppb).

only Cu^{2+} induced a prominent fluorescence enhancement, whereas very weak fluorescence variations were observed for the other metal ions. Additionally, these co-existent ions had negligible interfering effect on Cu^{2+} sensing by **4**, even when Na^+ , K^+ , Mg^{2+} , and Ca^{2+} were present at micromolar levels. Therefore, the excellent selectivity of **4** for Cu^{2+} over these physiological metal ions in aqueous media indicates its utility for a wide range of biological applications. Importantly, its high selectivity for Cu^{2+} over Cu^+ suggests that **4** might be used in tracking copper-related redox processes.

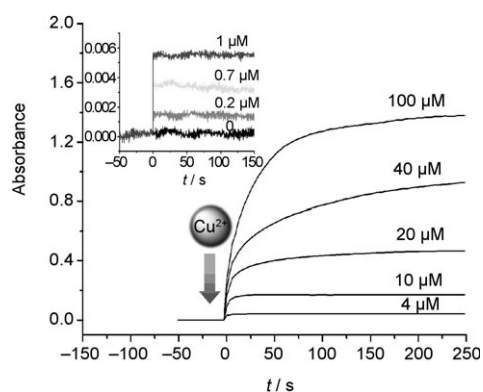


Figure 5. Time course of the response of **4** to different concentrations of Cu^{2+} . Absorbance at 555 nm was recorded in $20 \mu\text{M}$ **4** in $\text{CH}_3\text{CN}/\text{HEPES}$ (50 mM, pH 7.2, 3:7, v/v) solution.

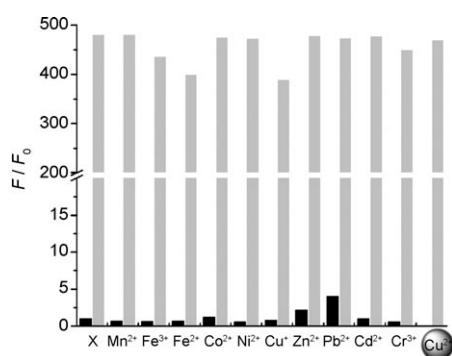


Figure 6. Fluorescence intensity changes (F/F_0) of $20 \mu\text{M}$ **4** upon the addition of various metal ions in $\text{CH}_3\text{CN}/\text{HEPES}$ (50 mM, pH 7.2, 3:7, v/v) solution. Dark bars represent the fluorescence response of **4** to the metal ion of interest (10 mM for K^+ , Na^+ , Ca^{2+} and Mg^{2+} ; $25 \mu\text{M}$ for Fe^{2+} and Cu^+ ; and $100 \mu\text{M}$ for other metal ions; X is a mixture of K^+ , Na^+ , Mg^{2+} and Ca^{2+}). Gray bars represent the subsequent addition of $100 \mu\text{M}$ Cu^{2+} to above solutions. Excitation and emission was at 510 and 580 nm, respectively.

Fluorescence imaging of intercellular Cu^{2+} : We proceeded to investigate the practical applicability of **4** as a Cu^{2+} probe in the fluorescence imaging of living cells. As determined by laser scanning confocal microscopy, staining HeLa cells with $5 \mu\text{M}$ **4** for 10 min at 25°C gave no intracellular fluorescence (Figure 7a). When the cells were supplemented with $50 \mu\text{M}$ CuCl_2 in the growth medium for 20 h at 37°C and then incubated with **4** under the same conditions, a significant fluorescence increase from the intracellular region was observed (Figure 7b). Control experiments on Cu^{2+} -supplemented cells without staining with **4** exhibited negligible background fluorescence (data not shown). Brightfield measurements after treatment with Cu^{2+} and **4** confirmed that the cells were viable throughout the imaging experiments (Figure 7c). The overlay of fluorescence and Brightfield images revealed that the fluorescence signals were localized in the perinuclear region of the cytosol (Figure 7d), indicating the subcellular distribution of Cu^{2+} which was internalized into the living cells from the growth medium.

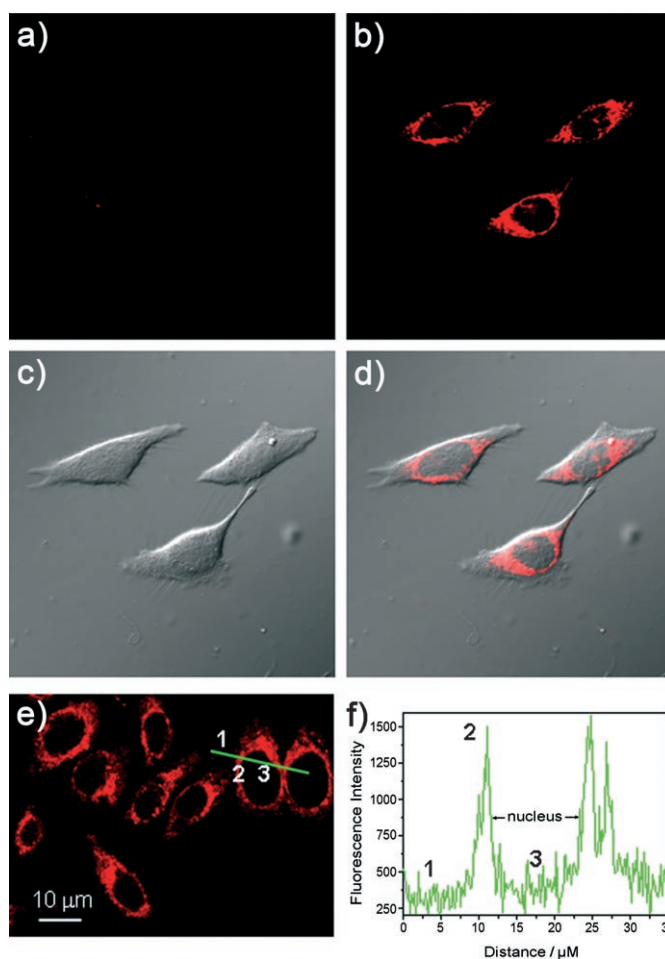


Figure 7. Confocal fluorescence and brightfield images of HeLa cells. a) Cells stained with $5 \mu\text{M}$ **4** for 10 min at 25°C . b) Cells supplemented with $50 \mu\text{M}$ CuCl_2 in the growth media for 20 h at 37°C and then incubated with $5 \mu\text{M}$ **4** for 10 min at 25°C . c) Brightfield image of cells shown in panel b. The overlay image of b) and c) is shown in d) ($\lambda_{\text{ex}} = 543 \text{ nm}$). e) Two-photon excited fluorescence image of Cu^{2+} supplemented HeLa cells stained with $5 \mu\text{M}$ **4** for 10 min at 25°C ($\lambda_{\text{ex}} = 880 \text{ nm}$). f) Fluorescence intensity profile across a HeLa cell shown in a).

We further explored the dose-dependent response of **4** to Cu^{2+} in live cells by fluorescence imaging of MCF-7 cells supplemented with different concentrations of Cu^{2+} . After incubation with $50 \mu\text{M}$ **4** for 30 min at 37°C , cells pretreated with $50 \mu\text{M}$ Cu^{2+} (for 20 h at 37°C) showed fluorescence exclusively in the perinuclear region of the cytosol, and cells supplemented with 100 or $200 \mu\text{M}$ Cu^{2+} exhibited more intense fluorescent signals that were located diffusely over the cytosol (see Figure S19 in the Supporting Information). In the control experiments, $50 \mu\text{M}$ **4** incubated cells without supplement with Cu^{2+} exhibited negligible background fluorescence (see Figure S19 in the Supporting Information). These results indicate that the presence of Cu^{2+} causes the fluorescence increase observed in cells. Furthermore, the cytotoxicity of the probe **4** was determined by trypan blue viability test (see Figure S20 in the Supporting Information). The viabilities of MCF-7 cells still retained 94.3 and 90.2%

after the incubation with 50 or 200 μM Cu^{2+} , respectively, and then staining with **4**; this suggests that most of the MCF-7 cells were viable in the fluorescence imaging experiments mentioned above. In the control experiments without staining with **4**, the cellular viabilities were 98.2 and 93.6% corresponding to the 50 or 200 μM Cu^{2+} -supplemented cells, respectively, further indicating that this Cu^{2+} fluorescent probe **4** can be considered to have low cytotoxicity. These results demonstrate that **4** can be used for monitoring Cu^{2+} within biological samples.

Compared with the single-photon related confocal fluorescent bioimaging technique, two-photon laser scanning microscopy (TPLSM) imaging has the advantages of high transmission at low incident intensity and reduced background cellular autofluorescence,^[27] thus has been widely used for the in vivo imaging in neuroscience.^[28] Because rhodamine B is a classical two-photon active dye,^[29] it is reasoned that chemodosimeter **4** may be used in two-photon imaging. Cu^{2+} -supplemented HeLa cells were stained with **4** under the same loading conditions; then, when excitation was provided at 880 nm, intense intracellular fluorescence signals at 550–650 nm were detected (Figure 7e). As shown in Figure 7f, quantization by line plots shows a signal-to-noise ratio (I_2/I_1) of 4.3 between cytoplasm (region 2) and background (region 1) and a ratio (I_2/I_3) of 3.5 between cytoplasm (region 2) and nucleus (region 3), further confirming the cytoplasmic distribution of intracellular Cu^{2+} . These facts reveal the potential utility of **4** as a Cu^{2+} -sensitive two-photon excited fluorescent probe for the in vivo bioimaging by TPLSM.

Conclusion

In conclusion, we have developed a rhodamine B derivative **4** and demonstrated its utility as a fluorescence turn-on chemodosimeter that responds stoichiometrically, rapidly, and highly sensitively to Cu^{2+} in aqueous media. The recognition process involves Cu^{2+} -promoted ring-opening, redox and hydrolysis reactions, which may be attributed to the highly electron-rich S atom in **4**. Comparable amplifications of the absorption and fluorescence signals were observed in its response towards Cu^{2+} , suggesting that chemodosimeter **4** effectively avoided the fluorescence quenching caused by the paramagnetic nature of Cu^{2+} . This chemodosimeter displayed very high sensitivity (detection limit ≤ 10 ppb), a rapid response time (≤ 1 min), and high selectivity for Cu^{2+} over other trace transition metal ions and abundant cellular cations. Moreover, confocal and two-photon fluorescence microscopy experiments have established the utility of **4** in monitoring Cu^{2+} within living cells and mapping its subcellular distribution. We anticipate that this probe will be of great benefit to biomedical researchers for studying the effects of Cu^{2+} in biological systems.

Experimental Section

General: *N*-(2-Hydroxyethyl)piperazine-*N'*-2-ethanesulfonic acid (HEPES) was purchased from Acros Organics. All other chemicals were purchased from Sigma-Aldrich and were used as received. TLC analyses were performed on silica gel 60 F₂₅₄. Column chromatographic purifications were carried out on silica gel (HG/T2354-92). NMR spectra were recorded on a Mercury Plus 400 MHz spectrometer (Varian Gemini-400). All chemical shifts are reported in the standard δ notation of parts per million. Mass spectra (EI) were measured on an MA1212 instrument under standard conditions. Electrospray ionization mass spectra (ESI-MS) were measured on a Micromass LCTTM system. Elemental analyses were performed on a VarioEL III O-Element Analyzer system. UV/Vis absorption spectra were recorded on a Shimadzu 3000 spectrophotometer. Fluorescence emission spectra were measured on an Edinburgh LFS920 luminescence spectrometer with a 1000 W xenon lamp. Luminescence quantum yields in solution were measured by using rhodamine B ($\Phi_F=0.69$ in ethanol)^[30] Samples for absorption and emission measurements were contained in 1 cm \times 1 cm quartz cuvettes as a reference. Deionized water was used to prepare all aqueous solutions. Solutions of Cu^+ , Hg^{2+} , Fe^{2+} , Mn^{2+} , Na^+ , K^+ , and Ca^{2+} were prepared from their chloride salts; solutions of Zn^{2+} , Cd^{2+} , Fe^{3+} , Pb^{2+} , Co^{2+} , Ni^{2+} , Cr^{3+} , Ag^+ , and Mg^{2+} were prepared from their nitrate salts. Solutions of Cu^{2+} were prepared from its chloride, nitrate, and sulfate salts. HEPES buffer solutions (pH 7.2) were prepared using 50 mM HEPES and the appropriate amount of NaOH. All spectroscopic measurements were performed in $\text{CH}_3\text{CN}/\text{HEPES}$ (50 mM, pH 7.2, 3:7, v/v) solution.

Synthesis of 4: According to previous literature reports^[16,21] rhodamine B hydrazide (**3**) was prepared and then characterized by its NMR and mass spectra. *n*-Butyl isothiocyanate (2.5 g, 22 mmol) was added to a solution of **3** (1.0 g, 2.2 mmol) in chloroform (10 mL). The mixture was then heated under reflux for 3 d. Thereafter, the solvent was evaporated under reduced pressure, and the crude product was purified by column chromatography (petroleum ether/ethyl acetate 4:1) to give **4** as a colorless solid (0.85 g, 68%). M.p. 106–109°C; ¹H NMR (400 MHz, CDCl_3 , 25°C, TMS): $\delta=0.786$ (t, $J=7.0$ Hz, 3H, C(=S)NHCH₂CH₂CH₂CH₃), 1.15 (m, 16H, NCH₂CH₃, C(=S)NHCH₂CH₂CH₂CH₃), 3.23 (q, $J=6.4$ Hz, 2H, C(=S)NHCH₂CH₂CH₂CH₃), 3.31 (q, $J=7.1$ Hz, 8H, NCH₂CH₃), 5.88 (t, $J=4.8$ Hz, 1H, C(=S)NHCH₂CH₂CH₂CH₃), 6.28 (d, $J=8.4$ Hz, 2H, xanthene-H), 6.40 (s, 3H, xanthene-H), 6.42 (s, 1H, xanthene-H), 6.75 (s, 1H, NHC(=S)NHCH₂CH₂CH₂CH₃), 7.23 (d, $J=7.6$ Hz, 1H, phenyl-H), 7.54 (m, 2H, phenyl-H), 7.98 ppm (d, $J=7.6$ Hz, 1H, phenyl-H); ¹³C NMR (400 MHz, CDCl_3 , 25°C, TMS): $\delta=12.8, 13.9, 20.1, 30.9, 44.6, 44.9, 67.0, 98.5, 104.6, 108.3, 124.0, 125.0, 127.8, 129.1, 129.3, 134.4, 149.4, 150.6, 154.4, 167.4, 183.1$ ppm; MS (EI): m/z (%): 571.5 (27) [M^+]; elemental analysis calcd (%) for C₃₃H₄₁N₅O₂S: C 69.32, H 7.23, N 12.25; found: C 69.25, H 7.48, N 12.50.

Synthesis of 5 from 4 upon addition of Hg²⁺: Mercury(II) perchlorate hydrate (0.18 g, 0.36 mmol) was added to a solution of **4** (0.10 g, 0.18 mmol) in CH_3CN (2 mL). The mixture was stirred at room temperature for 1 d. Thereafter, the solvent was removed under reduced pressure, and the crude product was purified by column chromatography ($\text{CHCl}_3/\text{MeOH}$ 6:1) to give **5** as a dark-purple solid (0.032 g, 33%). ¹H NMR (400 MHz, CDCl_3 , 25°C, TMS): $\delta=0.697$ (t, $J=7.2$ Hz, 3H, oxadiazole-N-CH₂CH₂CH₂CH₃), 1.07 (m, 2H, oxadiazole-N-CH₂CH₂CH₂CH₃), 1.25 (m, 14H, NCH₂CH₃, oxadiazole-N-CH₂CH₂CH₂CH₃), 2.84 (s, 2H, oxadiazole-N-CH₂CH₂CH₂CH₃), 3.55 (q, $J=7.1$ Hz, 8H, NCH₂CH₃), 6.78 (s, 2H, xanthene-H), 6.82 (d, $J=9.6$ Hz, 2H, xanthene-H), 7.05 (d, $J=9.2$ Hz, 2H, xanthene-H), 7.27 (m, 1H, Ar-H), 7.67 (m, 2H, Ar-H), 8.14 ppm (m, 1H, Ar-H); MS (EI): m/z (%): calcd for C₃₃H₄₀N₅O₂: 537.3 [$M-H$]⁺; found: 537.4.

Synthesis of 6 from 4 upon addition of Cu²⁺: Copper(II) nitrate hydrate (0.086 g, 0.36 mmol) was added to a solution of **4** (0.10 g, 0.18 mmol) in CH_3CN (2 mL). The mixture was stirred at room temperature for 10 min. Thereafter, the solvent was removed under reduced pressure, and the crude product was purified by column chromatography ($\text{CHCl}_3/\text{MeOH}$ 6:1) to give **6** as a dark-purple solid (0.021 g, 26%). ¹H NMR (400 MHz, CDCl_3 , 25°C, TMS): $\delta=1.29$ (t, $J=7.0$ Hz, 12H, NCH₂CH₃), 3.53 (q, $J=$

7.2 Hz, 8H, NCH_2CH_3), 6.70 (d, $J=2.4$ Hz, 2H, xantheno-H), 6.75 (dd, $J_1=9.6$ Hz, $J_2=2.4$ Hz, 2H, xantheno-H), 7.10 (d, $J=9.2$ Hz, 2H, xantheno-H), 7.19 (m, 1H, Ar-H), 7.67(m, 2H, Ar-H), 8.47 ppm (m, 1H, Ar-H); MS (EI): m/z (%): calcd for $C_{28}H_{31}N_2O_3$: 442.2 $[M-H]^+$; found: 442.3.

X-ray crystallographic analyses: A single crystal of **4** was mounted on a glass fiber and transferred to a Bruker SMART CCD area detector. Crystallographic measurements were made on a Bruker SMART CCD diffractometer, with σ scans and graphite-monochromated $MoK\alpha$ radiation ($\lambda=0.71073$ Å) at room temperature. The structure was solved by direct methods and refined by full-matrix least-squares on F^2 values using the program SHELXS-97.^[31] All non-hydrogen atoms were refined anisotropically. Hydrogen atoms were calculated in ideal geometries. For the full-matrix least-squares refinements [$I > 2\sigma(I)$], the unweighted and weighted agreement factors of $R1=\Sigma(F_o-F_c)/\Sigma F_o$ and $wR2=[\Sigma w(F_o^2-F_c^2)^2/\Sigma wF_o^4]^{1/2}$ were used.

Theoretical calculations: The structures of **1** and **4** were optimized using density functional theory (DFT) by the B3LYP method with the 3-21G** basis set. The contours of the HOMO and LUMO were plotted. The DFT calculations were performed using the Gaussian 03 program.^[32]

X-ray photoelectron spectroscopy analyses: An aqueous solution of copper(II) chloride (20 μ L, 0.44 mol L⁻¹; 0.0015 g, 0.009 mmol) was added to a solution of **4** (0.010 g, 0.018 mmol) in ethanol (1 mL). The mixture was stirred at room temperature for 10 min. Thereafter, the solvent was removed under reduced pressure, and the dark-purple product was used for XPS experiments. The measurements were carried out on a RBD upgraded PHI-5000C ESCA system (Perkin Elmer) with $MgK\alpha$ radiation ($h\nu=1253.6$ eV).

Procedures for metal-ion sensing: Stock solutions of the metal ions (2.5 mM) were prepared in deionized water, except for Cu^{2+} , which was dissolved in CH_3CN . A stock solution of **4** (1 mM) was also prepared in CH_3CN , and was then diluted to 20 μ M or 1 μ M with CH_3CN /HEPES (50 mM, pH 7.2, 3:7, v/v) solution. Titration experiments were performed by placing 2.5 mL of a solution of **4** (20 or 1 μ M) in a quartz cuvette of 1 cm optical path length, and then adding the Cu^{2+} or Hg^{2+} stock solution incrementally by means of a micro-pipette. Spectra were recorded 3 min after the addition. Test samples for selectivity experiments were prepared by adding appropriate amounts of metal ion stock solutions to 2.5 mL of a solution of **4** (20 μ M). In competition experiments, Cu^{2+} was added to solutions containing **4** and the other metal ions of interest. All test solutions were stirred for 1 min and then allowed to stand at room temperature for 30 min. For fluorescence measurements, excitation was provided at 510 nm, and emission was collected from 520 to 700 nm.

Cell culture: The cell lines HeLa and MCF-7 were provided by the Institute of Biochemistry and Cell Biology, SIBS, CAS (China). The HeLa cells were grown in MEM (modified Eagle's medium) supplemented with 10% FBS (fetal bovine serum) at 37°C and 5% CO_2 . The MCF-7 cells were grown in MEM (modified Eagle's medium) supplemented with 10% FBS (fetal bovine serum) and 1% insulin (10 mL/400 U) at 37°C and 5% CO_2 . Cells (5×10^8 L) were plated on 14 mm glass coverslips and allowed to adhere for 24 h. Experiments to assess Cu^{2+} uptake were performed over 20 h in the same medium supplemented with 50, 100, or 200 μ M $CuCl_2$.

Fluorescence imaging: Immediately before the experiments, cells were washed with PBS buffer, and then HeLa cells were incubated with 5 μ M **4** in PBS for 10 min at 25°C, while MCF-7 cells were incubated with 50 μ M **4** in PBS for 30 min at 37°C. Cell imaging was then carried out after washing the cells with PBS. Confocal fluorescence imaging was performed with an OLYMPUS IX81 laser scanning microscope and a 60 \times oil-immersion objective lens. Cells loaded with **4** were excited at 543 nm using an HeNe laser. Emission was collected from 550 to 650 nm. Two-photon fluorescence imaging was performed using an OLYMPUS BX61W1 laser scanning microscope and a 40 \times water-immersion objective lens. Two-photon fluorescence was excited by a Ti/sapphire femto-second laser source (Coherent Chameleon Ultra) set at 880 nm and an output power of 2 W, which corresponded to an average power of approximately 50 mW in the focal plane. Emission was collected from 550 to 650 nm.

Trypan blue viability test: MCF-7 cells (1×10^8 L) were plated on 14 mm glass coverslips and allowed to adhere for 24 h. Subsequently, cells were supplemented with 50 or 200 μ M $CuCl_2$ in the growth medium for 20 h at 37°C, and were incubated with 50 μ M **4** for 30 min at 37°C. After washing with PBS, 0.1% trypan blue solution was dropped onto the cells that adhered to the coverslips. Finally, viable (unstained by trypan blue) and non-viable (stained by trypan blue) cells were counted under a microscope. The cellular viability was calculated by the following formula: Viability (%) = total viable cells/total cells (viable and non-viable) \times 100.

Acknowledgements

The authors are thankful for the financial support from National Natural Science Foundation of China (20490210, 20501006 and 20775017), National High Technology Program of China (2006 AA03Z318), NCET-06-0353, Shanghai Science and Technology Community (06QH14002), Huo Yingdong Education Foundation (104012) and Shanghai Leading Academic Discipline Project (B108). We also thank Professor Cong-Jian Xu and Dr. Xiao-Yan Zhang for their helpful discussion.

- [1] a) M. C. Linder, M. Hazegh-Azam, *Am. J. Clin. Nutr.* **1996**, *63*, 797S-811S; b) R. Uauy, M. Olivares, M. Gonzalez, *Am. J. Clin. Nutr.* **1998**, *67*, 952S-959S.
- [2] a) D. J. Waggoner, T. B. Bartnikas, J. D. Gitlin, *Neurobiol. Dis.* **1999**, *6*, 221-230; b) C. Vulpe, B. Levinson, S. Whitney, S. Packman, J. Gitschier, *Nat. Genet.* **1993**, *3*, 7-13; c) P. C. Bull, G. R. Thomas, J. M. Rommens, J. R. Forbes, D. W. Cox, *Nat. Genet.* **1993**, *5*, 327-337.
- [3] K. J. Barnham, C. L. Masters, A. I. Bush, *Nat. Rev. Drug Discovery* **2004**, *3*, 205-214.
- [4] a) J. S. Valentine, P. J. Hart, *Proc. Natl. Acad. Sci. USA* **2003**, *100*, 3617-3622; b) L. I. Bruijn, T. M. Miller, D. W. Cleveland, *Annu. Rev. Neurosci.* **2004**, *27*, 723-749.
- [5] D. R. Brown, H. Kozlowski, *Dalton Trans.* **2004**, 1907-1917.
- [6] P. G. Georgopoulos, A. Roy, M. J. Yonone-Lioy, R. E. Opiekun, P. J. Lioy, *J. Toxicol. Environ. Health Part B* **2001**, *4*, 341-394.
- [7] a) Z. L. Harris, J. D. Gitlin, *Am. J. Clin. Nutr.* **1996**, *63*, 836S-841S; b) I. H. Scheinberg, I. Sternlieb, *Am. J. Clin. Nutr.* **1996**, *63*, 842S-845S.
- [8] For reviews of cell imaging, see: a) R. Y. Tsien, *Methods Cell Biol.* **1989**, *30*, 127-156; b) C. Brownlee, *Trends Cell Biol.* **2000**, *10*, 451-457; c) W. R. Zipfel, R. M. Williams, W. W. Webb, *Nat. Biotech.* **2003**, *21*, 1369-1377; d) D. J. Stephens, V. J. Allan, *Science* **2003**, *300*, 82-86; e) J. Lichtman, J. A. Conchello, *Nat. Methods* **2005**, *2*, 910-919; f) B. N. G. Giepmans, S. R. Adams, M. H. Ellisman, R. Y. Tsien, *Science* **2006**, *312*, 217-224.
- [9] For recent examples of imaging specific species in cells, see: a) M. H. Lim, S. J. Lippard, *Acc. Chem. Res.* **2007**, *40*, 41-51; b) E. W. Miller, O. Tulyanthan, E. Isacoff, C. J. Chang, *Nat. Chem. Biol.* **2007**, *3*, 263-267; c) K. H. Xu, B. Tang, G. W. Yang, Y. Yang, L. G. An, *Chem. Eur. J.* **2007**, *13*, 1411-1416; d) S. Kenmoku, Y. Urano, H. Kojima, T. Nagano, *J. Am. Chem. Soc.* **2007**, *129*, 7313-7318; e) M. Zhang, M. X. Yu, F. Y. Li, M. W. Zhu, M. Y. Li, Y. H. Gao, L. Li, Z. Q. Liu, J. P. Zhang, D. Q. Zhang, T. Yi, C. H. Huang, *J. Am. Chem. Soc.* **2007**, *129*, 10322-103213.
- [10] For recent examples, see: a) H. Komatsu, T. Miki, D. Citterio, T. Kubota, Y. Shindo, Y. Kitamura, K. Oka, K. Suzuki, *J. Am. Chem. Soc.* **2005**, *127*, 10798-10799; b) G. Farruggia, S. Iotti, L. Prodi, M. Montalti, N. Zaccheroni, P. B. Savage, V. Trapani, P. Sale, F. I. Wolf, *J. Am. Chem. Soc.* **2006**, *128*, 344-350; c) R. M. Sánchez-Martín, M. Cuttle, S. Mittoo, M. Bradley, *Angew. Chem.* **2006**, *118*, 5598-5600; *Angew. Chem. Int. Ed.* **2006**, *45*, 5472-5474; d) H. M. Kim, C. Jung, B. R. Kim, S. Y. Jung, J. H. Hong, Y. G. Ko, J. L. Kyoung, B. R. Cho, *Angew. Chem.* **2007**, *119*, 3530-3533; *Angew. Chem. Int. Ed.* **2007**, *46*, 3460-3463.

- [11] For reviews, see: a) K. Kikuchi, K. Komatsu, T. Nagano, *Curr. Opin. Chem. Biol.* **2004**, *8*, 182–191; b) N. C. Lim, H. C. Freake, C. Brückner, *Chem. Eur. J.* **2005**, *11*, 38–49, and references therein.
- [12] For recent examples, see: a) K. Komatsu, K. Kikuchi, H. Kojima, Y. Urano, T. Nagano, *J. Am. Chem. Soc.* **2005**, *127*, 10197–10204; b) E. M. Nolan, J. W. Ryu, J. Jaworski, R. P. Feazell, M. Sheng, S. J. Lippard, *J. Am. Chem. Soc.* **2006**, *128*, 15517–15528; c) X. A. Zhang, K. S. Lovejoy, A. Jasanoff, S. J. Lippard, *Proc. Natl. Acad. Sci. USA*, **2007**, *104*, 10780–10785.
- [13] a) X. J. Peng, J. J. Du, J. L. Fan, J. Y. Wang, Y. K. Wu, J. Z. Zhao, S. G. Sun, T. Xu, *J. Am. Chem. Soc.* **2007**, *129*, 1500–1501; b) W. M. Liu, L. W. Xu, R. L. Sheng, P. F. Wang, H. P. Li, S. K. Wu, *Org. Lett.* **2007**, *9*, 3829–3832.
- [14] L. Zeng, E. W. Miller, A. Pralle, E. Y. Isacoff, C. J. Chang, *J. Am. Chem. Soc.* **2006**, *128*, 10–11.
- [15] Q. W. He, E. W. Miller, A. P. Wong, C. J. Chang, *J. Am. Chem. Soc.* **2006**, *128*, 9316–9317.
- [16] M. Zhang, Y. H. Gao, M. Y. Li, M. X. Yu, F. Y. Li, L. Li, M. W. Zhu, J. P. Zhang, T. Yi, C. H. Huang, *Tetrahedron Lett.* **2007**, *48*, 3709–3712.
- [17] a) Z. C. Zhang, D. Wu, X. F. Guo, X. H. Qian, Z. Lu, Q. Xu, Y. Y. Yang, L. P. Duan, Y. K. He, Z. Feng, *Chem. Res. Toxicol.* **2005**, *18*, 1814–1820; b) S. K. Ko, Y. K. Yang, J. S. Tae, I. J. Shin, *J. Am. Chem. Soc.* **2006**, *128*, 14150–14155; c) S. H. Yoon, E. W. Miller, Q. W. He, P. H. Do, C. J. Chang, *Angew. Chem.* **2007**, *119*, 6778–6781; *Angew. Chem. Int. Ed.* **2007**, *46*, 6658–6661; d) H. Yang, Z. G. Zhou, K. W. Huang, M. X. Yu, F. Y. Li, T. Yi, C. H. Huang, *Org. Lett.* **2007**, *9*, 4729–4732.
- [18] For fluorescence “turn-off” Cu²⁺ sensors, see: a) D. Y. Sasaki, D. R. Shnek, D. W. Pack, F. H. Arnold, *Angew. Chem.* **1995**, *107*, 994–996; *Angew. Chem. Int. Ed. Engl.* **1995**, *34*, 905–907; b) A. Torrado, G. K. Walkup, B. Imperiali, *J. Am. Chem. Soc.* **1998**, *120*, 609–610; c) P. Grandini, F. Mancini, P. Tecilla, P. Scrimin, U. Tonellato, *Angew. Chem.* **1999**, *111*, 3247–3250; *Angew. Chem. Int. Ed.* **1999**, *38*, 3061–3064; d) G. Klein, D. Kaufmann, S. Schürch, J. L. Reymond, *Chem. Commun.* **2001**, 561–562; e) M. Boiocchi, L. Fabbrizzi, M. Licchelli, D. Sacchi, M. Vázquez, C. Zampa, *Chem. Commun.* **2003**, 1812–1813; f) Y. Zheng, J. Orbulescu, X. Ji, F. M. Andreopoulos, S. M. Pham, R. M. Leblanc, *J. Am. Chem. Soc.* **2003**, *125*, 2680–2686; g) B. C. Roy, B. Chandra, D. Hromas, S. Mallik, *Org. Lett.* **2003**, *5*, 11–14; h) N. Shao, Y. Zhang, S. M. Cheung, R. H. Yang, W. H. Chan, T. Mo, K. A. Li, F. Liu, *Anal. Chem.* **2005**, *77*, 7294–7303; i) S. H. Kim, J. S. Kim, S. M. Park, S. K. Chang, *Org. Lett.* **2006**, *8*, 371–374.
- [19] For fluorescence “turn-on” Cu²⁺ sensors, see: a) Q. Wu, E. V. Anslyn, *J. Am. Chem. Soc.* **2004**, *126*, 14682–14683; b) Z. C. Xu, Y. Xiao, X. H. Qian, J. N. Cui, D. W. Cui, *Org. Lett.* **2005**, *7*, 889–892; c) Z. C. Wen, R. Yang, H. He, Y. B. Jiang, *Chem. Commun.* **2006**, 106–108; d) R. Martinez, F. Zapata, A. Caballero, A. Espinosa, A. Tarraga, P. Molina, *Org. Lett.* **2006**, *8*, 3235–3238; e) Y. Xiang, A. J. Tong, P. Y. Jin, Y. Ju, *Org. Lett.* **2006**, *8*, 2863–2866; f) H. Yang, Z. Q. Liu, Z. G. Zhou, E. X. Shi, F. Y. Li, Y. K. Du, T. Yi, C. H. Huang, *Tetrahedron Lett.* **2006**, *47*, 2911–2914; g) J. W. Liu, Y. Lu, *J. Am. Chem. Soc.* **2007**, *129*, 9838–9839.
- [20] a) A. V. Varnes, R. B. Dodson, E. L. Whery, *J. Am. Chem. Soc.* **1972**, *94*, 946–950; b) J. A. Kemlo, T. M. Shepherd, *Chem. Phys. Lett.* **1977**, *47*, 158–162.
- [21] V. Dujols, F. Ford, A. W. Czarnik, *J. Am. Chem. Soc.* **1997**, *119*, 7386–7387.
- [22] For metal ions, see: a) G. Hennrich, H. Sonnenschein, U. Resch-Genger, *J. Am. Chem. Soc.* **1999**, *121*, 5073–5074; b) B. Liu, H. Tian, *Chem. Commun.* **2005**, 3156–3158; c) J. V. Ros-Lis, M. D. Marcos, R. Martínez-Máñez, K. Rurack, J. Soto, *Angew. Chem.* **2005**, *117*, 4479–4482; *Angew. Chem. Int. Ed.* **2005**, *44*, 4405–4407. For other analytes, see: d) C. A. Roeschlaub, N. L. Maidwell, R. Rezaei, P. G. Sammes, *Chem. Commun.* **1999**, 1637–1638; e) F. Sancenón, A. B. Descalzo, R. Martínez-Máñez, M. A. Miranda, J. Soto, *Angew. Chem.* **2001**, *113*, 2710–2713; *Angew. Chem. Int. Ed.* **2001**, *40*, 2640–2643; f) T. H. Kim, T. M. Swager, *Angew. Chem.* **2003**, *115*, 4951–4954; *Angew. Chem. Int. Ed.* **2003**, *42*, 4803–4806; g) F. Sancenón, R. Martínez-Máñez, M. A. Miranda, M. J. Seguí, J. Soto, *Angew. Chem.* **2003**, *115*, 671–674; *Angew. Chem. Int. Ed.* **2003**, *42*, 647–650; h) F. Tanaka, N. Mase, C. F. Barbas, *Chem. Commun.* **2004**, 1762–1763; i) G. J. Mohr, *Chem. Eur. J.* **2004**, *10*, 1082–1090.
- [23] Y. K. Yang, K. J. Yook, J. S. Tae, *J. Am. Chem. Soc.* **2005**, *127*, 16760–16761.
- [24] Crystal data for C₃₃H₄₁N₅O₂S: *F*_w = 571.78, monoclinic (*P*2₁(*n*)), *a* = 12.129(12), *b* = 12.326(13), *c* = 23.44(2) Å, *α* = 90, *β* = 101.390(14), *γ* = 90°, *V* = 3435(6) Å³, *ρ*_{calcd} = 1.185 g cm⁻³, *Z* = 4, *μ* = 0.133 mm⁻¹, *R*₁ [*I* > 2σ(*I*)] = 0.0887, *wR*₂ [*I* > 2σ(*I*)] = 0.1862, *R*₁ (all data) = 0.2609, *wR*₂ (all data) = 0.2702, GOF = 0.894. CCDC 649657 contains the supplementary crystallographic data for this paper. These data can be obtained free of charge from The Cambridge Crystallographic Data Centre via www.ccdc.cam.ac.uk/data_request/cif.
- [25] a) J. Y. Kwon, Y. J. Jang, Y. J. Lee, K. M. Kim, M. S. Seo, W. Nam, J. Yoon, *J. Am. Chem. Soc.* **2005**, *127*, 10107–10111; b) Y. Xiang, A. J. Tong, *Org. Lett.* **2006**, *8*, 1549–1552; c) H. Zhang, Z. H. Qian, L. Xu, F. F. Yuan, L. D. Lan, J. G. Xu, *Org. Lett.* **2006**, *8*, 859–861; d) J. Mao, L. N. Wang, W. Dou, X. L. Tang, Y. Yan, W. S. Liu, *Org. Lett.* **2007**, *9*, 4567–4570.
- [26] A. Natarajan, Y. H. Guo, H. Arthanari, G. Wagner, J. A. Halperin, M. Chorev, *J. Org. Chem.* **2005**, *70*, 6362–6368.
- [27] K. D. Belfield, K. J. Schafer, Y. Liu, X. B. Ren, E. W. Van Stryland, *J. Phys. Org. Chem.* **2000**, *13*, 837–849.
- [28] K. Svoboda, R. Yasuda, *Neuron* **2006**, *50*, 823–839.
- [29] C. Xu, W. W. Webb, *J. Opt. Soc. Am. B* **1996**, *13*, 481–491.
- [30] N. Filipescu, G. W. Mushrush, C. R. Hurt, N. McAvoy, *Nature* **1966**, *211*, 960.
- [31] G. M. Sheldrick, SHELXS-97: *SHELXTL-Plus V5.1 software Reference Manual*, Bruker AXS, Madison, WI, **1997**.
- [32] Gaussian 03, Revision B05, M. J. Frisch, G. W. Trucks, H. B. Schlegel, G. E. Scuseria, M. A. Robb, J. R. Cheeseman, J. A. Montgomery, T. Vrevenjr, K. N. Kudin, J. C. Burant, J. M. Millam, S. S. Iyengar, J. Tomasi, V. Barone, B. Mennucci, M. Cossi, G. Scalmani, N. Rega, G. A. Petersson, H. Nakatsuji, M. Hada, M. Ehara, K. Toyota, R. Fukuda, J. Hasegawa, M. Ishida, T. Nakajima, Y. Honda, O. Kitao, H. Nakai, M. Klene, X. Li, J. E. Knox, H. P. Hratchian, J. B. Cross, V. Bakken, C. Adamo, J. Jaramillo, R. Gomperts, R. E. Stratmann, O. Yazyev, A. J. Austin, R. Cammi, C. Pomelli, J. W. Ochterski, P. Y. Ayala, K. Morokuma, G. A. Voth, P. Salvador, J. J. Dannenberg, V. G. Zakrzewski, S. Dapprich, A. D. Daniels, M. C. Strain, O. Farkas, D. K. Malick, A. D. Rabuck, K. Raghavachari, J. B. Foresman, J. V. Ortiz, Q. Cui, A. G. Baboul, S. Clifford, J. Cioslowski, B. B. Stefanov, G. Liu, A. Liashenko, P. Piskorz, I. Komaromi, R. L. Martin, D. J. Fox, T. Keith, M. A. Al-Laham, C. Y. Peng, A. Na-nayakkara, M. Challacombe, P. M. W. Gill, B. Johnson, W. Chen, M. W. Wong, C. Gonzalez, J. A. Pople, Gaussian, Wallingford, CT, **2003**.

Received: January 2, 2008

Revised: April 3, 2008

Published online: July 7, 2008